JGR Oceans

RESEARCH ARTICLE
10.1029/2019JC015839

Special Section:
Years of the Maritime Continent

Intraseasonal Kelvin Waves in the Equatorial Indian Ocean and Their Propagation into the Indonesian Seas

Kandaga Pujiana[1,2] **and Michael J. McPhaden**[1]

[1]NOAA Pacific Marine Environmental Laboratory, Seattle, WA, USA, [2]Faculty of Earth Sciences and Technology, Bandung Institute of Technology, Bandung, Indonesia

Abstract Intraseasonal oceanic variations in the Indian Ocean are prominent mode of variability affecting evolution of the Indian Ocean Dipole, the semiannual Wyrtki jets, and the Indonesian throughflow. This study describes the structure and propagation of wind-forced intraseasonal Kelvin waves along the equator in the Indian Ocean and their penetration into the Indonesian seas. For this purpose, we use an unprecedented multiyear (2004–2016) moored velocity time series data set from the equatorial central and eastern Indian Ocean, moored time series from Lombok, Makassar, and Ombai straits; satellite altimetry, and other oceanic and atmospheric data products. The waves are generated by zonal wind fluctuations with periods of approximately 20–90 days. They propagate eastward along the equator at speeds close to that of a second baroclinic mode (with estimates ranging between 1.3 and 1.7 ms^{-1} depending on method) and have an exponential latitudinal decay scale away from the equator of ~250 km. Phase also propagates upward, implying downward energy propagation, consistent with wind energy source at the surface. As the waves encounter the coast of Sumatra, they partially reflect into Rossby waves that radiate energy westward back into the ocean interior. Some wave energy also propagates southward along the coasts of Sumatra and Java and can be traced into Lombok, Ombai, and Makassar straits at lags of about 2–3 weeks. The implications of these results for understanding variability in the Indian Ocean and its connectivity with the Indonesian seas are discussed.

Plain Language Summary We investigate Indian Ocean equatorial Kelvin waves on weekly to monthly timescales and their propagation into the Indonesian seas. For this purpose, we use ocean current velocity data from an unprecedented number of moorings during 2004–2016, plus satellite data and other data sets. Consistent with theoretical expectations, the wave structures decay exponentially away from the equator to the north and south, with a decay scale of approximately 250 km. The phase of the zonal current variations propagates eastward and upward consistent with eastward and downward energy propagation expected for Kelvin waves forced by surface winds. When the waves encounter the west coast of Sumatra, they partially reflect into Rossby waves that propagate westward back into the interior of the ocean. Some energy also continues poleward as coastal waves along Sumatra and Java. These waves eventually make their way into Lombok, Ombai, and Makassar straits in the Indonesian seas, affecting the velocity there. We discuss the implications of these results for understanding broader regional circulation patterns in the Indian Ocean.

Key Points:
- Observed equatorial Indian Ocean intraseasonal variations are consistent with Kelvin wave theory
- Zonal velocity and sea level propagate eastward at ≈1.5 ms^{-1} and are latitudinally symmetric with a 250-km decay scale about the equator
- Kelvin waves continue along the coasts of Java and Sumatra, making their way into the Indonesian seas through Lombok and Ombai straits

Supporting Information:
- Supporting Information S1

Correspondence to:
K. Pujiana,
kandaga.pujiana@noaa.gov

Citation:
Pujiana, K., & McPhaden, M. J. (2020). Intraseasonal Kelvin waves in the equatorial Indian ocean and Their propagation into the Indonesian seas. *Journal of Geophysical Research: Oceans, 125*, e2019JC015839. https://doi.org/10.1029/2019JC015839

Received 5 NOV 2019
Accepted 13 APR 2020
Accepted article online 17 APR 2020

1. Introduction

Intraseasonal fluctuations are a prominent mode of variability in the equatorial Indian Ocean. Sengupta et al. (2001) found energetic intraseasonal variations in observed subsurface zonal velocity (u) across the central-eastern part of the basin. Masumoto et al. (2005) reported that the amplitude of near-surface zonal velocity at 30- to 60-day periods was significantly larger than that on semiannual timescales observed in the eastern equatorial Indian Ocean. Meridional currents (v), though weaker than zonal currents, also exhibit pronounced intraseasonal variations in the equatorial Indian Ocean, particularly at periods of 10–20 days (Nagura & McPhaden, 2014; Sengupta et al., 2004; Smyth et al., 2015). The flow of water from the Pacific Ocean to the Indian Ocean through the Indonesian seas, known as the Indonesian throughflow (ITF), also exhibits energetic intraseasonal variability. For example, in Lombok and Ombai straits (Figure 1a), Sprintall et al. (2009) reported prominent 30- to 60-day oscillations in the ITF. Pujiana et al. (2009) also described significant intraseasonal oscillations in the ITF in Makassar Strait.

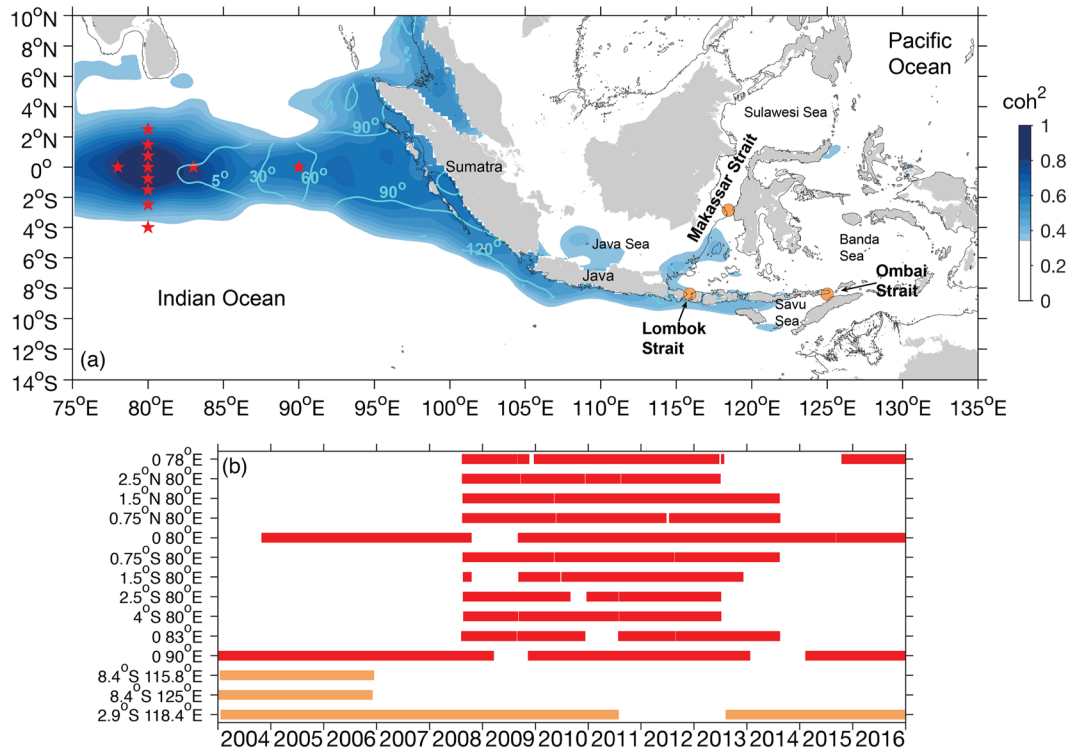

Figure 1. Mooring sites, respectively, marked as red stars and brown circles in the central-eastern Indian Ocean and Indonesian seas region (a) and observational period of the moorings (b). Shades of the blue color and cyan contours in (a) respectively illustrate squared coherence amplitudes and phases relative to the sea level anomaly (η) at 0°, 80.5° E and that in the region of interest, averaged over the intraseasonal frequency band (comprising periods of roughly 20–90 days). Satellite-derived η data between 2004 and 2016 are used to determine the coherence amplitudes and phases. Amplitudes lower than the 95% significance level are masked. Phase increasing to the east indicates eastward propagation. Gray contours show the 100-m isobath.

Previous studies have proposed various mechanisms for intraseasonal horizontal current variations in the equatorial Indian Ocean, with wind forcing as the primary cause of 30- to 60-day oscillations in near-surface u (Han et al., 2001; Iskandar & McPhaden, 2011; McPhaden, 1982). The wind partly derives from the Madden-Julian Oscillation (MJO), a dominant source of intraseasonal variability in the tropical atmosphere (Yoneyama et al., 2013; Zhang, 2013). Iskandar and McPhaden (2011), using data from moorings at 0°, 80.5° E and 0°, 90° E (Figure 1a), suggested that Kelvin waves account for the 30- to 60-day variations in upper ocean u. Instabilities that arise from Rossby wave mean flow interactions also contribute to 30- to 50-day variations of u in the upper 150 m of the central Indian Ocean (Sengupta et al., 2001). As for v, wind-forced mixed Rossby gravity waves are the dominant source of biweekly variations in cross-equatorial current in the Indian Ocean.

Once generated, equatorial waves affect sea level and ocean currents along wave characteristics away from the generation area. Iskandar et al. (2005), using satellite-derived sea level anomaly (η) data, posited connectivity between intraseasonal sea level variations along the equator and the southern coast of Sumatra and Java (Figure 1a) via Kelvin waves. The coastally trapped Kelvin waves propagate to the east along the southern coast of Java into Lombok Strait, Savu Sea, and Ombai Strait, resulting pronounced intraseasonal variability in sea level and horizontal currents there (Arief & Murray, 1996; Drushka et al., 2010; Schiller et al., 2010; Sprintall et al., 2010; Zhou & Murtugudde, 2010).

Durland and Qiu (2003) theoretically demonstrated that coastal Kelvin waves along the southern coast of Java could penetrate Lombok Strait (Figure 1a), despite the strait's narrow width compared to the local Rossby radius. Syamsudin et al. (2004), employing a 1.5-layer ocean model, also showed that a substantial fraction of the coastal Kelvin wave energy penetrates into Lombok Strait. Applying a linear wind-forced wave

model adapted from Kessler et al. (1995), Drushka et al. (2010) described how Kelvin waves originating in the equatorial Indian Ocean between 75 and 100° E account for intraseasonal along-strait velocity variations observed in Lombok and Ombai straits during 2004–2006. To the north of Lombok Strait in Makassar Strait, Pujiana et al. (2013) documented upward phase propagation in intraseasonal velocity variations related to propagating waves. Eddies that have a signature on intraseasonal timescales are also present in Makassar Strait (Pujiana et al., 2012)

This study builds on previous investigations of intraseasonal equatorial Kelvin waves in the Indian Ocean and their propagation into the Indonesian seas, using a unique collection of in situ horizontal current data from 14 moorings (Figure 1a), along with satellite data and reanalysis products. Our analysis is based on the most comprehensive set of moored velocity data records available today in the Indian Ocean, which for the first time allows detailed definition of the meridional structure of directly measured intraseasonal zonal velocity variations. This information provides additional dynamical constraints on the interpretation of the data in terms of Kelvin wave theory, in conjunction with satellite-derived sea surface height and surface geostrophic velocity. Finally, the connectivity of equatorial Kelvin waves with fluctuations on intraseasonal timescales in the Indonesian seas is further explored.

This paper proceeds with section 2 describing data and methods to classify Kelvin wave events. Section 3 discusses the meridional and vertical structures and dispersion characteristics of Kelvin waves in the equatorial Indian Ocean. Assessments of Kelvin waves propagation from the equatorial Indian Ocean into the Indonesian seas follow in section 4. We conclude with a summary and discussion.

2. Data and Methods

2.1. Data

2.1.1. In Situ Measurements

Meridional and vertical structures of Kelvin waves in the Indian Ocean are derived from hourly u collected by upward looking Acoustic Doppler Current Profilers (ADCPs) deployed from an array of subsurface moorings at 78° E, 80.5° E, 83° E, and 90° E in the equatorial Indian Ocean (Figure 1a). The ADCPs were part of the Research Moored Array for African-Asian-Australian Monsoon Analysis and Prediction (RAMA) (McPhaden et al., 2009, 2015). The equatorial RAMA ADCPs at 80.5° E and 90° E have recorded the velocities since October 2004 and November 2000, respectively, while the rest of the ADCPs were operational between August 2008–December 2013 (Figure 1b) (McPhaden et al., 2015; Nagura & McPhaden, 2016). Because of contamination of the velocity measurements from backscatter off the surface, we focused on the observed u between 30 and 250 m at 5-m vertical intervals.

Propagation of Indian Ocean Kelvin waves into the Indonesian seas is inferred from hourly along-strait velocity data obtained from moorings as part of ITF measurements in Lombok, Makassar, and Ombai straits (Figure 1a) (Gordon et al., 2010; Sprintall et al., 2009; Pujiana et al., 2019). The ITF mooring in Makassar Strait has been operational since January 2004, while those in Lombok and Ombai straits were operational during January 2004–December 2006 (Figure 1b). Similar to the RAMA moored velocity data, the near-surface velocity data from the ITF moorings were discarded. We analyzed the along-strait velocity by combining u and v that extend from 50 to 250 m in Lombok Strait and to 750 m in Makassar and Ombai straits. Since the along-strait axis in Makassar and Lombok straits aligns more with the north-south direction, we label the along-strait velocity there as v' and that in Ombai Strait as u'.

The hourly horizontal current data from the RAMA and ITF moorings were daily averaged and then band-pass filtered with cut-off frequencies of 0.0111–0.05 cycle day^{-1} (20–90 days), resulting in daily average time series of intraseasonal variability. Compared to the variance attributed to the horizontal current varying in a period band of 2–360 days, intraseasonal fluctuations on average account for about half of the variance, based on spectral analyses of depth-averaged u in the equatorial Indian Ocean and along-strait velocity in the Indonesian seas.

Major gaps in the daily averages of horizontal currents, such as at 0°, 80.5° E during October 2008–August 2009 (Figure 1b), were filled using data from nearby moorings via linear regression methods (Johnson & McPhaden, 1993). McPhaden et al. (2015) used similar gap filling methods, which were validated by comparing filled time series with observed time series for periods when no gaps actually existed. In Makassar

Strait, where no adjacent moorings existed, the gap of missing data during August 2011–July 2013 was left unfilled. Minor gaps with a length up to a few days between deployments were filled by linear interpolation.

Complementing the moored horizontal currents, profiles of temperature (T) and salinity (S) from Argo profilers, made available by the international Argo project, and from shipboard Conductivity-Temperature-Depth (CTD) casts in the vicinity of the moorings were analyzed. Aided by Argo- and CTD-derived T and S profiles, we computed Brunt-Väisällä frequency (N) profiles near the moorings useful for our analysis in assessing the background stratification conditions in which a Kelvin wave propagates.

2.1.2. Satellite-Derived and Reanalysis Data

Besides point-based measurements from the RAMA and ITF moorings, we analyzed satellite-derived surface currents, wind stress (τ), and η over the Indian Ocean and Indonesian maritime continent to provide insights into connectivity between Kelvin waves in the Indian Ocean and the Indonesian seas. We used the daily, 0.25° latitude × 0.25° longitude gridded τ and η data respectively from the near real-time Institut Francais de Recherche pour l′exploitation de la Mer product (Bentamy et al. 2002) and Archiving, Validation and Interpretation of Satellite Oceanographic data (Ducet et al. 2000). We also used 5-day averages on a 1° × 1° grid from the Ocean Surface Current Analysis Real Time (OSCAR) product (Bonjean & Lagerloef, 2002). To be consistent with other satellite-sourced datasets, the 5-day averages OSCAR data were interpolated to daily resolution. As with the moored data, the τ, η, and OSCAR surface current data were band-pass filtered to emphasize 20- to 90-day intraseasonal oscillations.

2.2. Classifying Kelvin Wave Events

Equatorial oceanic waves are trapped within several degrees of the equator and account for horizontal current and η variations across a broad frequency range. The zonal direction at which wave phase propagates, either eastward or westward, depends on the frequency of the wave. At intraseasonal periods between 20 and 90 days, Kelvin waves exhibit eastward phase propagation, while Rossby and mixed Rossby gravity waves propagate westward.

Applying a complex empirical orthogonal function (CEOF) method to the intraseasonal η averaged between 2° N–2° S along the equator in the Indian Ocean shows that the phase of the first two CEOF modes, accounting for 58% and 14% of the variance respectively, increases from west to east (Figure S1b, supporting information), indicative of eastward propagation. A linear fit to the phase structure indicates that a dominant fraction of intraseasonal η variance along the equator propagates eastward with an average phase speed between 1.0 ± 0.2 ms^{-1} (CEOF mode 2) and 1.8 ± 0.2 ms^{-1} (CEOF mode 1) (Figure S1b), which falls within a range of theoretical phase speeds for low baroclinic Kelvin waves inferred from normal mode decomposition of density stratification (Nagura & McPhaden, 2010a). In contrast, the phase structure of the third CEOF mode accounting for 8% of intraseasonal η variance decreases to the east along the equator, implying westward propagation with a phase speed range of 0.96 ± 0.1 ms^{-1}. Therefore, the first two CEOF modes likely capture the Kelvin wave signal in intraseasonal η along the equator, while the third mode likely represents low-frequency Rossby waves. Note that the phase speeds are for intraseasonal η oscillating at the central period of 55 days, and the respective uncertainties denote the 95% confidence intervals.

Based on the amplitude (Figure S1a) and principal component time series of the first CEOF mode, we reconstruct η (referred to as η_r) and then classify Kelvin wave events as events which exhibit continuous eastward propagation with $|\eta_r| \geq 2$ cm along the equator from 80.5° E or further west. We found 65 downwelling Kelvin wave ($\eta_r > 0$) and 57 upwelling Kelvin wave ($\eta_r < 0$) events during 2004 - 2016 (Figure S1c). We depict the general features of the Kelvin waves identifiable from η_r for each Kelvin wave group, with lag 0 day marking the time when the absolute magnitude of η_r is maximum at 80.5° E (right panel of Figure 2). The composites clearly illustrate propagation of η_r along the equator from western to the eastern Indian Ocean for both Kelvin wave groups.

Composite plots of intraseasonal zonal wind stress (τ^x), inferred from τ^x averaged between 2° N and 2° S along the equatorial Indian Ocean, for each Kelvin wave group show that westerly wind stress generates downwelling Kelvin waves, while easterly wind stress generates upwelling Kelvin waves (left panel of Figure 2). Westerly (easterly) wind stress peaks over the western basin about 5 days before η_r is maximum (minimum) at 80.5° E for the downwelling (upwelling) Kelvin wave. Intraseasonal westerly wind stress traverses eastward overlying the downwelling Kelvin wave (Figure 2a, right panel), whereas easterly wind

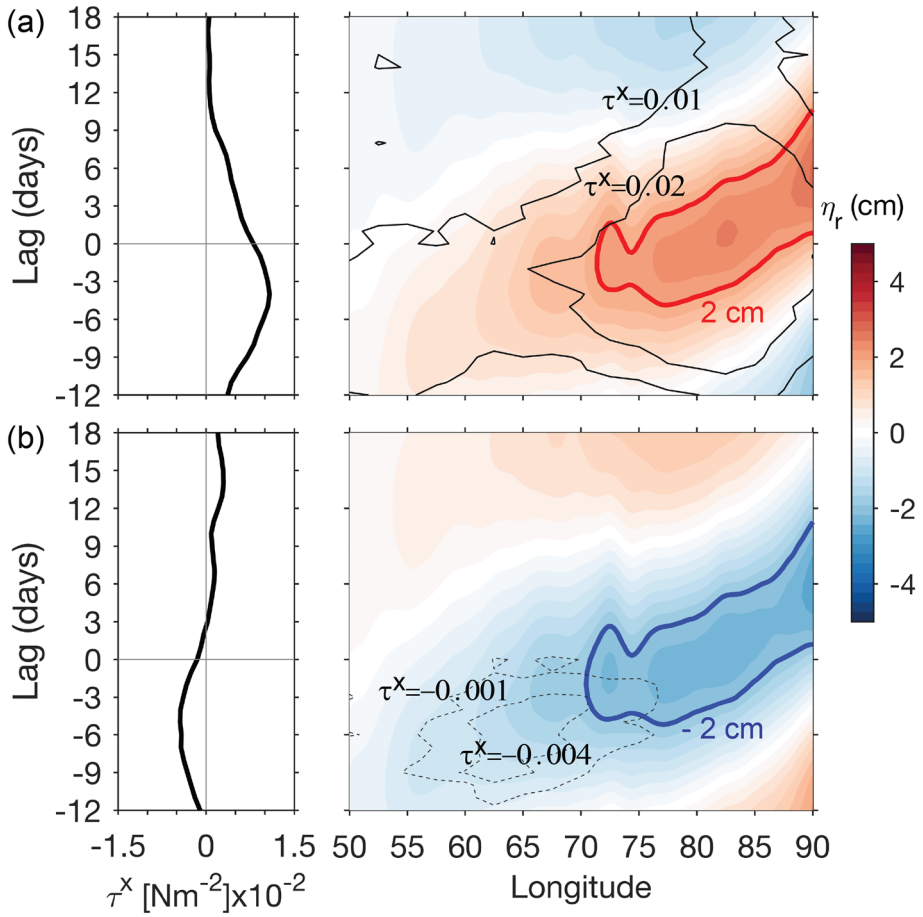

Figure 2. Composites of equatorial intraseasonal τ^x (left) averaged over longitude between 50 and 75° E and reconstructed η (η_r, right) attributed to the downwelling (a) and upwelling (b) Kelvin waves events identifiable in the equatorial Indian Ocean during 2004–2016. Lag = 0 marks the time when η_r attains its maximum (downwelling Kelvin waves) or minimum (upwelling Kelvin waves) magnitude at 80.5° E. Black contours on the time-longitude plots of η_r denote τ^x. Positive (negative) τ^x values indicate westerly (easterly) wind stress.

stress prevailing over the upwelling Kelvin wave does not appear to propagate eastward. The eastward propagating westerly wind stress is likely attributable to the MJO and may impact the evolution of the Kelvin wave over the central and eastern Indian Ocean, consistent with previous studies (Iskandar & McPhaden, 2011; Yan et al., 2012; Zhou & Murtugudde, 2010). However, the extent to which the local intraseasonal winds affect the Kelvin wave is not apparent from the composite analysis as the composite plots show no notable difference in zonal evolution between the downwelling and upwelling Kelvin waves (Figure 2, right panel). Therefore, we will henceforth discuss structures and transmission of the downwelling Kelvin wave for the rest of the paper, with the results implicitly applying to the upwelling Kelvin wave. Note that using the first two CEOF modes rather than just the first CEOF to reconstruct intraseasonally band-passed η does not significantly change our results.

2.3. CEOF of Horizontal Currents

To capture the vertical structure of Kelvin waves from the moored horizontal current, we decomposed the moored horizontal current data into their orthogonal functions and associated principal component time series using a CEOF method, adopting a similar technique implemented in Iskandar and McPhaden (2011). The focus of our analysis will be on the first CEOF mode that represents on average about 70% variances of intraseasonal u from the RAMA moorings and along-strait velocity from the ITF moorings.

We reconstructed the intraseasonal velocities using the amplitude of the orthogonal function and principal component time series of the first CEOF mode at all moorings and present a subset of the reconstructed velocities at 80.5° E, 90° E, Lombok, and Makassar straits over 2005–2008 in Figure 3.

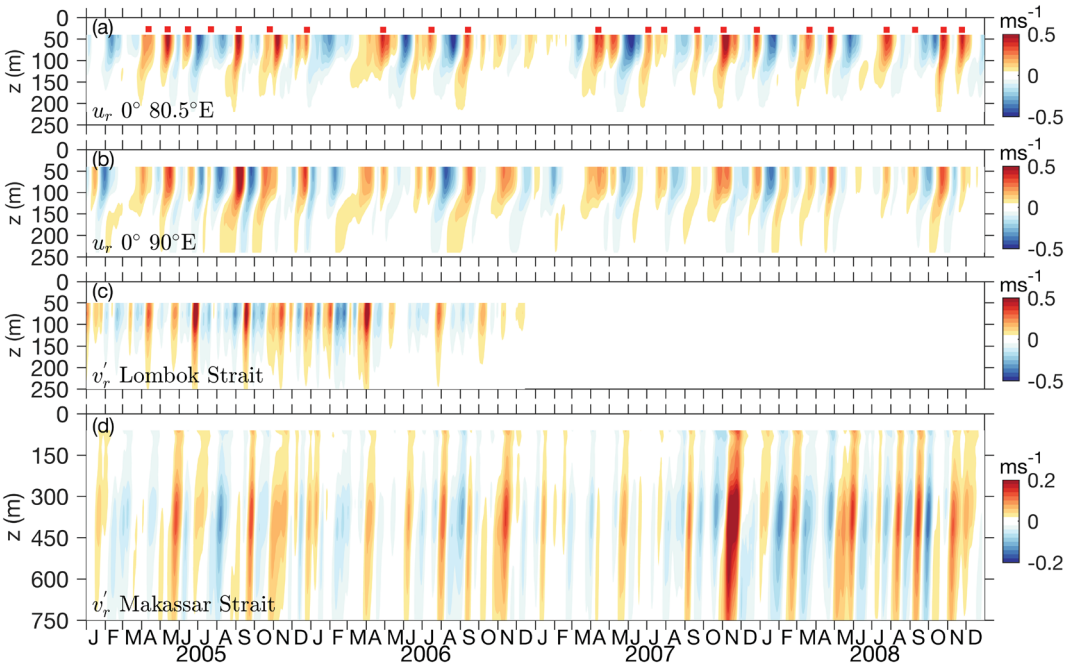

Figure 3. Reconstructed velocities based on the first CEOF mode of intraseasonal zonal velocity observed at (a) 0°, 80.5° E and (b) 0°, 90° E and along-strait velocity in (c) Lombok Strait and (d) Makassar Strait during the 2005–2008 period. Positive values indicate eastward velocity along the equator and northward along-strait velocities. Red boxes in (a) mark Kelvin wave events during the respective period identifiable from the reconstructed intraseasonal η_r at 0°, 80.5° E as discussed in the text.

3. Kelvin Wave Structure and Propagation

3.1. Meridional Structure

The unprecedented number of RAMA ADCP moorings concurrently operating during August 2008–July 2013 along 80.5° E (Figure 1) provides an opportunity to document Kelvin wave meridional structures for comparison with wave theory. Of 65 downwelling Kelvin wave events observed throughout the observational period, there were 22 passages of the downwelling Kelvin wave along the equator during August 2008–July 2013 (Figure S1c). For each of the Kelvin wave passages, we determined the arrival time of the maximum η_r (presumably represents Kelvin wave peak) at 80.5° E and then quantified the magnitude of reconstructed u (u_r) averaged within the upper 220 m observed at eight different mooring locations along 80.5° E. The upper (30 m) and lower (220 m) limits for these averages were the shallowest and deepest depths for which consistently good data were available from the ADCPs.

The magnitude of the depth-averaged u_r associated with the downwelling Kelvin wave events decays away from the equator and shows a Gaussian latitudinal dependence (Figure 4, red dots), consistent with a Kelvin wave meridional structure. Using the least-squares technique, we fitted the u_r meridional structure to the theoretical Kelvin wave solution on an equatorial β plane

$$u_r(y) = u_r(0)e^{\left(\frac{-\beta y^2}{2c}\right)}, \quad (1)$$

where $\beta = 2.3\times 10^{-11}$, y is latitude, $u_r(0)$ is the reconstructed zonal current at the equator, and c is phase speed. By allowing both $u_r(0)$ and c to vary, the best least-squares fit exhibits an exponential function with $u_r \sim 0.1$ ms^{-1} and $c \sim 1.4 \pm 0.3$ ms^{-1} (red solid line in Figure 4). Based on vertical mode decomposition of Argo profiler-derived N^2 profiles in the tropical Indian Ocean, Nagura and McPhaden (2010a) reported that Kelvin wave horizontal phase speeds for the first four vertical modes are 2.5, 1.5, 0.9, and 0.5 ms^{-1}, respectively. Thus, the estimated phase speed of 1.4 ms^{-1} most closely approximates the theoretical phase speed of the second baroclinic mode Kelvin wave (Figure 4). Given the estimated phase speed, we argue that u_r is trapped near the equator with a decay scale ($L = \sqrt{\frac{c}{\beta}}$) of 247 ± 25 km. Changing the extent across which the depth averaging of u_r is performed does not change this result significantly. Note also that the magnitude of

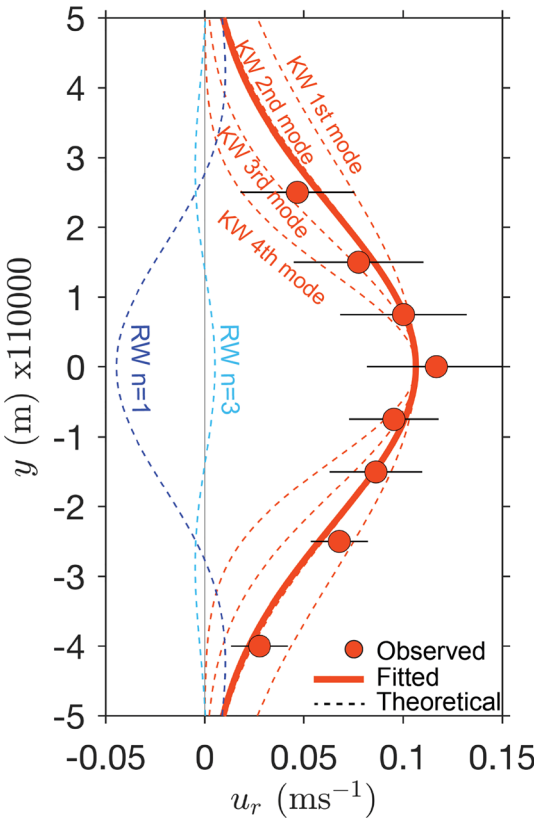

Figure 4. Meridional structure of reconstructed intraseasonal u (u_r) along 80.5° E associated with downwelling Kelvin wave events during August 2008–July 2013. Red dots show the magnitudes of depth-averaged u_r in the upper 220 m attributed to the Kelvin wave events observed by the RAMA moorings, solid red line is the least-squares fit of the depth-averaged u_r using an exponential function of (1), red dashed lines denote meridional structures of u_r associated with the first four baroclinic mode Kelvin waves, and blue dashed lines show projections of the first two symmetric meridional mode Rossby waves based on the phase speed, c, inferred from the least-squares exponential fit for the Kelvin wave. Horizontal lines indicate the standard deviation of the depth-averaged u_r.

$u_r(0)$ reasonably agrees well with that inferred from the full record at the 80.5° E mooring during October 2004–December 2016, which is on average 0.13 ± 0.04 ms^{-1}.

Low-frequency Rossby wave appears less influential in explaining the moored u_r. The projections of the exponential least-squares fit to the meridional structures of u_r, attributed to the first two hemispherically symmetric mode Rossby waves ($n = 1$ and 3), can be represented by equation (2) (e.g., Boulanger & Menkes, 1995)

$$u_r^n(y) = R_u^n(u_r.R_u^n) \tag{2}$$

with $R_u^n = \sqrt{\frac{n(n+1)}{2(2n+1)}}\left(\frac{\psi_{n+1}}{\sqrt{n+1}} - \frac{\psi_{n-1}}{\sqrt{n}}\right)$ and $\psi_n(y) = \frac{1}{\sqrt{2^n n!\sqrt{\pi}}} e^{\frac{-y^2}{2}} H_n(y)$. $H_n(y)$ are the Hermite polynomials with y scaled by $L = \sqrt{c/\beta}$, with c =1.4 ms^{-1}. Rossby waves do not appear to reasonably account for the meridional structure estimated from the observations (dashed blue curves in Figure 4).

To further examine the meridional structure of intraseasonal variations near the equator, we analyzed the meridional structure of band-pass filtered η along 80.5° E and its respective zonal surface geostrophic anomaly during the Kelvin wave passages identifiable between August 2008 and July 2013. Assuming a quasi-geostrophic balance in the meridional direction, the zonal surface geostrophic current off the equator (u_g) is given by $f u_g = -g\frac{\partial \eta}{\partial y}$, with f and g denoting Coriolis and gravity acceleration, respectively, while on the equator, $\beta u_g = -g\frac{\partial^2 \eta}{\partial y^2}$ applies. We used a center difference scheme to estimate the first and second derivatives of η.

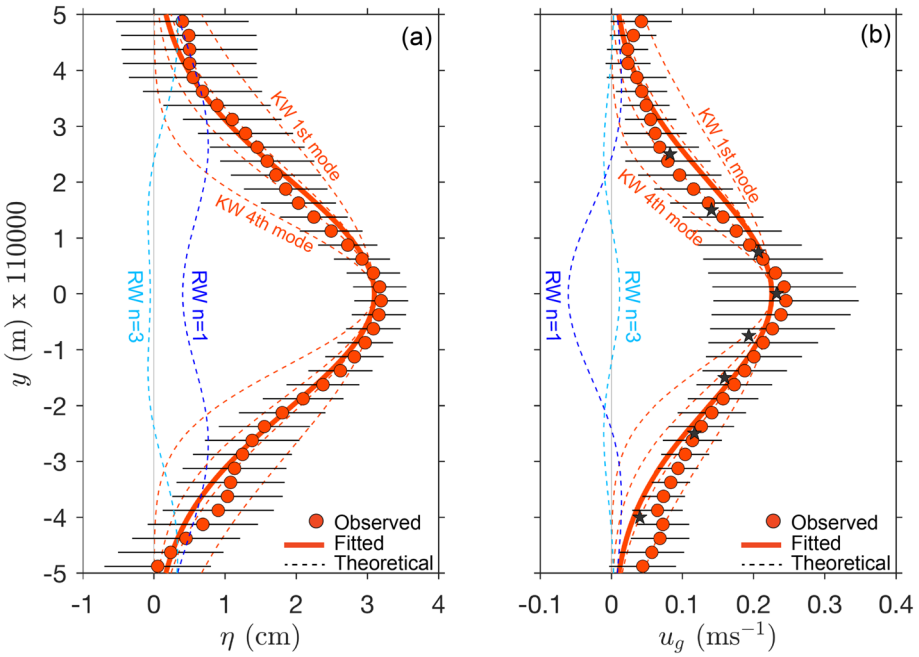

Figure 5. Meridional structures of intraseasonal (a) η and (b) u_g along 80.5° E associated with the Kelvin wave events during the period of August 2008–July 2013 inferred from the satellite-derived data. Red dots show the average magnitudes, solid red lines are the least-squares exponential fits of the observed magnitudes, red dashed lines indicate meridional structures for the first four baroclinic mode Kelvin waves, blue dashed lines show projections of the first two hemispherically symmetric Rossby wave modes (n = 1 and 3) based on c, inferred from the least-squares exponential fit for the Kelvin wave, and horizontal lines indicate the standard deviation. Stars on (b) denote the average values of u_r at the surface, linearly extrapolated from the u_r observed between 40 and 100 m.

Observed intraseasonal η along 80.5° E averaged over the course of the Kelvin wave passages show a meridional structure that is approximately symmetric about the equator (Figure 5a). Using the least-squares method, we fit the observed mean meridional η structure to an exponential function $\eta(y) = \eta(0)e^{\frac{-\beta y^2}{2c}}$ attributed to the theoretical cross-equatorial structure of the equatorial Kelvin wave and found the best exponential fit with $\eta(0)$ and c of 3.1 cm and 1.3 ± 0.2 ms^{-1}, respectively. Based on the inferred c, we argue that the cross-equatorial structure of the second vertical mode of the Kelvin wave best replicates the observed meridional structure of intraseasonal η, consistent with the results deduced from u_r. Similar to u_r, projections of the observed η to the first two symmetric modes of the Rossby wave, which are respectively given by

$$\eta^n(y) = R^n_\eta(\eta.R^n_\eta), \tag{3}$$

do not substantially account for the measured maximum η on the equator, with $R^n_\eta = \sqrt{\frac{n(n+1)}{2(2n+1)}}(\frac{\psi_{n+1}}{\sqrt{n+1}} + \frac{\psi_{n-1}}{\sqrt{n}})$.

As expected, the meridional structure of zonal surface geostrophic flow averaged during the Kelvin wave passages follows that of η, with a maximum at the equator and decaying exponentially off the equator (Figure 5b). Like in u_r and η, the best least-squares exponential fit to the observed mean u_g mimics the meridional structure of the second baroclinic Kelvin wave mode with the inferred c of 1.3 ± 0.2 ms^{-1}. The mean surface values of u_r, linearly extrapolated from the observed u_r between 40 and 100 m and then averaged for the Kelvin wave events, are reasonably in agreement with the u_g meridional structure derived from the best exponential fit, signifying the Gaussian latitudinal dependence of the Kelvin wave. The decay scale of η and u_g is about 238 km, reasonably close to that of u_r.

A distinguishing feature of equatorial Kelvin waves versus Rossby waves is the relationship between zonal velocity and surface pressure, which is proportional to $g\,\eta$ (Yu & McPhaden, 1999). For the Kelvin wave, the ratio of the pressure to the zonal velocity is proportional to c, while for a Rossby wave it is $c/(2n+1)$, where n is an integer ≥1. Based on the magnitudes of the best exponential fit of η and u_g shown in Figure 5, we find that the ratio of surface pressure to zonal current at the equator is about 1.4 ± 0.1 ms^{-1} which is essentially identical to the value inferred from fitting the moored zonal velocities to a meridional Gaussian structure.

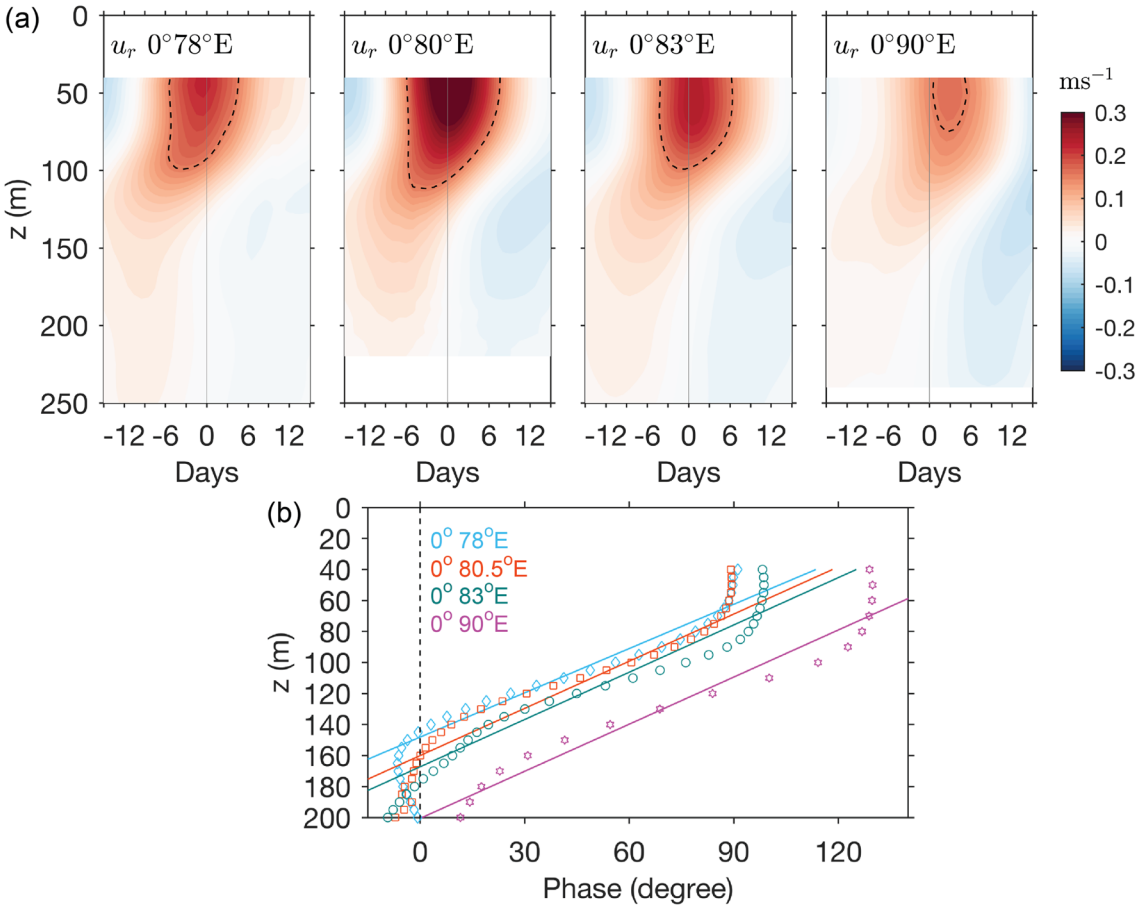

Figure 6. Composites of u_r based on the first CEOF mode of intraseasonal u attributed to Kelvin wave events observed during August 2008–July 2013 at RAMA equatorial moorings; dashed contours mark $u_r = 0.15$ ms^{-1}. Lag values are relative to 40 m zonal currents at 0°, 80.5° E. (b) CEOF phases of u_r; values increasing to the east and upward indicate eastward and upward phase propagation. The phase at each mooring site is referenced to that at 0°, 80.5° E at 160 m. Color-coded lines show the linear least-squares fits to the CEOF phases across depths beneath 50 m.

This further indicates the predominance of Kelvin waves in accounting for the variability observed along the equator.

3.2. Vertical Structure

As for the meridional structure, we assess the vertical structure of the Kelvin wave from the reconstructed zonal velocity, focusing on the RAMA moorings along the equator. We derived a composite of u_r attributed to Kelvin wave passages at each of the moorings, with day = 0 marking the time when η attributed to the Kelvin wave passages is maximum at 80.5° E. The composite shows a gradual Kelvin wave phase shift in u_r at the equatorial moorings (Figure 6a), with deeper levels leading shallower levels.

Upward phase propagation is indicative of downward energy propagation (McCreary, 1984), so that the pronounced vertical phase shift observed from the moored zonal velocity suggests an energy source at the surface, namely, zonal wind forcing. Note that the composited vertical structure at 0°, 80.5° E and 0°, 90° E, derived from 22 Kelvin wave events identifiable between August 2008 and July 2013, does not significantly differ from that composed of 61 Kelvin wave events identifiable during November 2004–December 2016 (Figure S2). This illustrates that the structure of Kelvin wave characteristics is relatively stationary.

To further explore the vertical phase propagation and hence quantitatively determine its speed, we analyzed the phase profile inferred from the first CEOF mode of intraseasonal u. Consistent with the vertical phase shift shown in Figure 6a, the phase profile exhibits a trend of decreasing phase with depth, indicative of upward phase propagation (Figure 6b). The rate of the phase decrease is smaller between the shallowest depth resolved by the ADCPs and 80 m compared to deeper depths. The relatively uniform phase near the

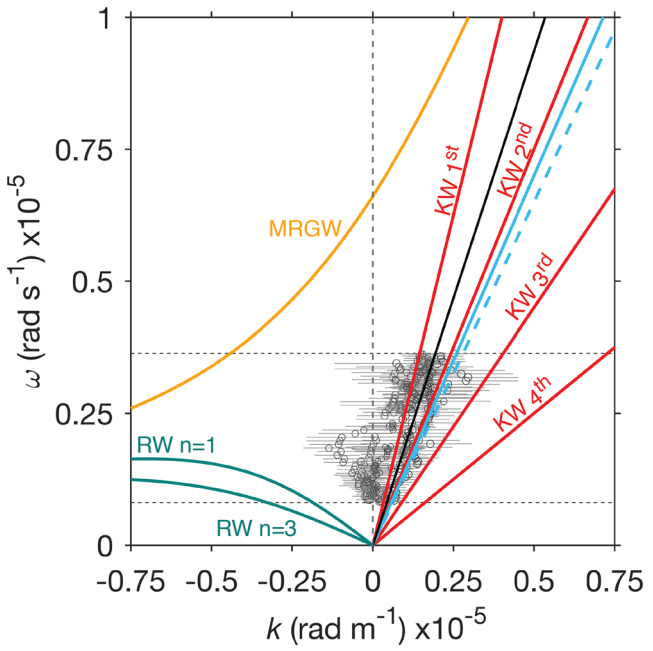

Figure 7. Theoretical dispersion curves of equatorial waves and observed dispersion relation. Circles indicate wavenumber-frequency plot inferred from coherence analysis of u_r at different moorings along the equatorial Indian Ocean, and color-coded solid lines indicate the first four baroclinic modes of Kelvin waves (red), the first two meridional modes of low-frequency Rossby waves (green), and the mixed Rossby gravity wave (orange). Black line shows the linear least-squares fit of the black dots, blue lines mark the estimated dispersion curves with c =1.3 ms^{-1} (dashed line) and c =1.4 ms^{-1} (solid line) inferred from the best least-squares fits of u_r, η, and u_g along 80.5° E as discussed in the text. Rossby wave and mixed Rossby gravity wave dispersion curves are based on c = 1.4 ms^{-1}. Horizontal gray lines denote 95% confidence level for the wavenumber-frequency estimates, based on a Monte Carlo method. Horizontal dashed black lines mark the intraseasonal frequency band.

surface likely indicates the direct impact of wind stress forcing on the near-surface u, in agreement with the finding of Iskandar and McPhaden (2011), who found a strong, in-phase relationship between τ^x and u over 40–100 m depths on intraseasonal timescales.

We can estimate the speed of the upward phase propagation from the slope of a linear least-squares fit to the vertical variation of the CEOF phase (Figure 6b). These fits indicate upward propagation at speeds of 3.4 ± 0.2 m day^{-1} to 15.2 ± 0.7 m day^{-1} at periods between 20 and 90 days. At a period of 55 days, where the spectral peak of the depth-averaged u_r time series occurs, the upward phase speed is 5.5 ± 0.3 m day^{-1}. Iskandar and McPhaden (2011) also reported an intraseasonal spectral peak centered at around 55 days, characterizing zonal current along the equatorial Indian Ocean.

As in previous Indian Ocean dynamical studies (Luyten & Roemmich, 1982; McPhaden, 1982; Nagura & McPhaden, 2016), we invoke the Wentzel-Kramers-Brillouin approximation to examine vertically propagating wave features. Assuming the magnitude of N^2 changes vertically at a slower rate than the vertical wavelength of the wave, a Kelvin wave with a certain frequency should propagate vertically at an angle and with a speed inversely proportional to the buoyancy frequency. The slope (θ) at which a linear equatorial Kelvin wave propagates in a longitude (x) - depth (z) plane is given as $\theta = \frac{dz}{dx} = \frac{\omega}{N}$ (McCreary, 1984). In the time-longitude domain, the slope is equivalently represented as $\frac{dz}{dt}\frac{dt}{dx} = \frac{\omega}{N}$, implying that the upward phase propagation speed ($\frac{dz}{dt}$) is proportional to ω, $\frac{dx}{dt}$ (equivalent to c), and N^{-1}. By specifying $N = 2.6\times 10^{-2}$ s^{-1} (the average value of buoyancy frequency across depth between 80 and 200 m in the equatorial Indian Ocean between 75 and 90° E inferred from Argo profilers and shipboard CTD casts near the RAMA moorings), assigning $c = 1.3$ ms^{-1} as derived from the least-squares fit to the meridional structures of zonal current and sea level anomaly shown in Figures 4 and 5, the upward phase speed of the theoretical intraseasonal Kelvin wave ranges between 3.5 and 15.6 m day^{-1} for ω in the 20- to 90-day period band. Thus, the upward phase speeds estimated from the CEOF phase variations of u_r are in agreement with the theoretical vertical phase speeds for Kelvin wave.

The vertical structure of u_r attributed to the Kelvin wave events at different longitudes along the equator shows not only upward phase propagation but also eastward phase propagation, with the structure observed at 0°, 90° E lagging by a few days that at 0°, 80.5° E (Figure 6a). To further explore Kelvin wave characteristics from these observations, we examined the frequency-zonal wavenumber distribution of zonal current variations. We deduced zonal wavenumber from the reconstructed velocity at locations separated by a distance (d) to yield coherence amplitude and phase (α) at a discrete frequency (ω) within the intraseasonal frequency band. Using the coherence phase information with the respective amplitude exceeding the 95% significance level, we estimated the zonal wavenumber (k) as $k(\omega) = \frac{\alpha(\omega)}{d}$.

Applying coherence analysis of the reconstructed velocities at different mooring locations in the wave guide results in a zonal wavenumber-frequency scatter plot. The wavenumber-frequency plot (circles in Figure 7) illustrates that the inferred wavenumber magnitude from the observations is mostly positive, implying eastward propagation from the equatorial Indian Ocean to the Indonesian seas. Within the framework of the theoretical dispersion curves of equatorial waves, the inferred wavenumber-frequency estimates in the intraseasonal frequency band are distinctively different from those of low-frequency Rossby waves and the mixed Rossby gravity wave. The observed $\omega - k$ scatter generally clusters around the theoretical dispersion curves for the gravest three baroclinic Kelvin wave modes, with the least-squares fit to the $\omega - k$ estimates falling in between the dispersion curves for the first two baroclinic modes. The horizontal phase speed inferred from the fit is 1.7 ± 0.4 ms^{-1}, roughly equivalent to that inferred from the meridional structure of

u_r, η, and u_g along 80.5° E. We will next discuss the propagation of these equatorial Kelvin waves into the coastal zone and the Indonesian seas.

3.3. Transmission into Indonesian Seas

We have shown that moored and satellite-derived intraseasonal η and u data along 80.5° E exhibit Kelvin wave meridional structures associated with the gravest vertical modes, most notably the second mode. The moored u data at four different locations along the equator between 78 and 90° E show inherent Kelvin wave characteristics such as upward and eastward phase propagation. Intraseasonal sea level variations at 0°, 80.5° E are also coherent with those along the coasts of Sumatra and Java, with the phase of the coherent sea level increasing towards the coasts that implies propagation into the Indonesian seas (Figure 1a). Is the wave signature emanating from the equatorial Indian Ocean still identifiable in the Indonesian seas?

As a first approach to address this question, we made a composite of η and surface currents for all Kelvin wave events identifiable during August 2008–July 2013 over the region of interest. Extending the period of analysis to 2004–2016 to account for more Kelvin wave events yields comparable results. The composite shows that a downwelling intraseasonal Kelvin wave, marked by eastward u and elevated η within a latitude range of 4° N–4° S, propagates eastward along the equator and then poleward once it encounters the coast of Sumatra (Figure 8).

Focusing on its transmission in the Southern Hemisphere, the wave pulse propagates along the southern coast of Java and farther eastward into Ombai Strait as a coastally trapped downwelling Kelvin wave, hugging the coastlines on its left and increasing η along the way. This is consistent with the result of Iskandar et al. (2005), using coastal pressure gauge-recorded η during January 1995–April 1997, who reported that intraseasonal variations in η along the Sumatra and Java coasts were of equatorial Indian Ocean origin.

In addition to the coastally trapped wave component propagating along the coastlines of the Indonesian islands, the downwelling Kelvin wave of equatorial Indian Ocean origin also generates reflected downwelling Rossby waves, marked by elevated η and anticyclonic surface currents centered at around 5° N and 5° S off the coast of Sumatra.

The satellite-derived intraseasonal η data, however, do not clearly capture the transmission of the coastally trapped wave into the interior of the Indonesian seas. The composite of η shows a weaker sign of propagation from the southern coast of Java to Makassar Strait, compared to that from the southern coast of Java to Ombai Strait. Aided by η data from a few units of coastal pressure gauge deployed along the coast of Sumatra and Java and in Makassar Strait, Iskandar et al. (2005) suggested that Indian Ocean Kelvin wave did not penetrate into Makassar Strait. There is no continuous coastline between Lombok Strait to Makassar Strait, but the Java Sea with an average depth of between 50 and 100 m connects the two straits (Figure 8). The coastline discontinuity might lead to a weaker signature of the coastally trapped wave in sea level.

We also analyzed the moored velocity data in the Indonesian straits to track the wave transmission into the Indonesian seas. The composite of the moored velocity, based on the data from the ITF and equatorial RAMA moorings between October 2004 and December 2006, shows that the Indian Ocean downwelling Kelvin wave forces northward along-strait velocity ($v_r' > 0$) in Lombok and Makassar straits and eastward along-strait velocity ($u_r' > 0$) in Ombai Strait, with the velocity consistently exhibiting upward phase propagation (Figure 9a). Theoretically, upward phase propagation is indicative of downward energy propagation, and upward phase propagation is observed at all sites. We note that the maximum velocity observed at 0°, 80.5° E, Lombok Strait, and Makassar Strait occurs respectively near surface, 75 m, and 350 m (Figure 9a). This indicates that the Kelvin wave transfers energy from the surface downward as it propagates away from its generation region in the equatorial Indian Ocean. Extended data observed over the course of October 2004–July 2011 and August 2013–December 2016 in Makassar Strait reveal a similar response of the along-strait velocity to passage of downwelling Kelvin waves (Figure S3).

Compared to intraseasonal zonal velocity in the equatorial Indian Ocean, the reconstructed along-strait velocity in the Indonesian straits exhibits a steeper $\frac{dz}{dt}$, implying a faster speed of upward phase propagation (Figure 9a). Based on CEOF phases of the along-strait velocity (Figure 9b), we determined that the speed of upward phase propagation for a Kelvin wave with a period of 55 days, the spectral peak period of the velocity time series, in the Indonesian straits is 31.5 ± 7 m day^{-1}, about six times faster than the upward phase speed in the equatorial Indian Ocean. Why the upward phase speed is faster in the Indonesian straits than in the equatorial Indian Ocean remains unknown, but background stratification may partly account for

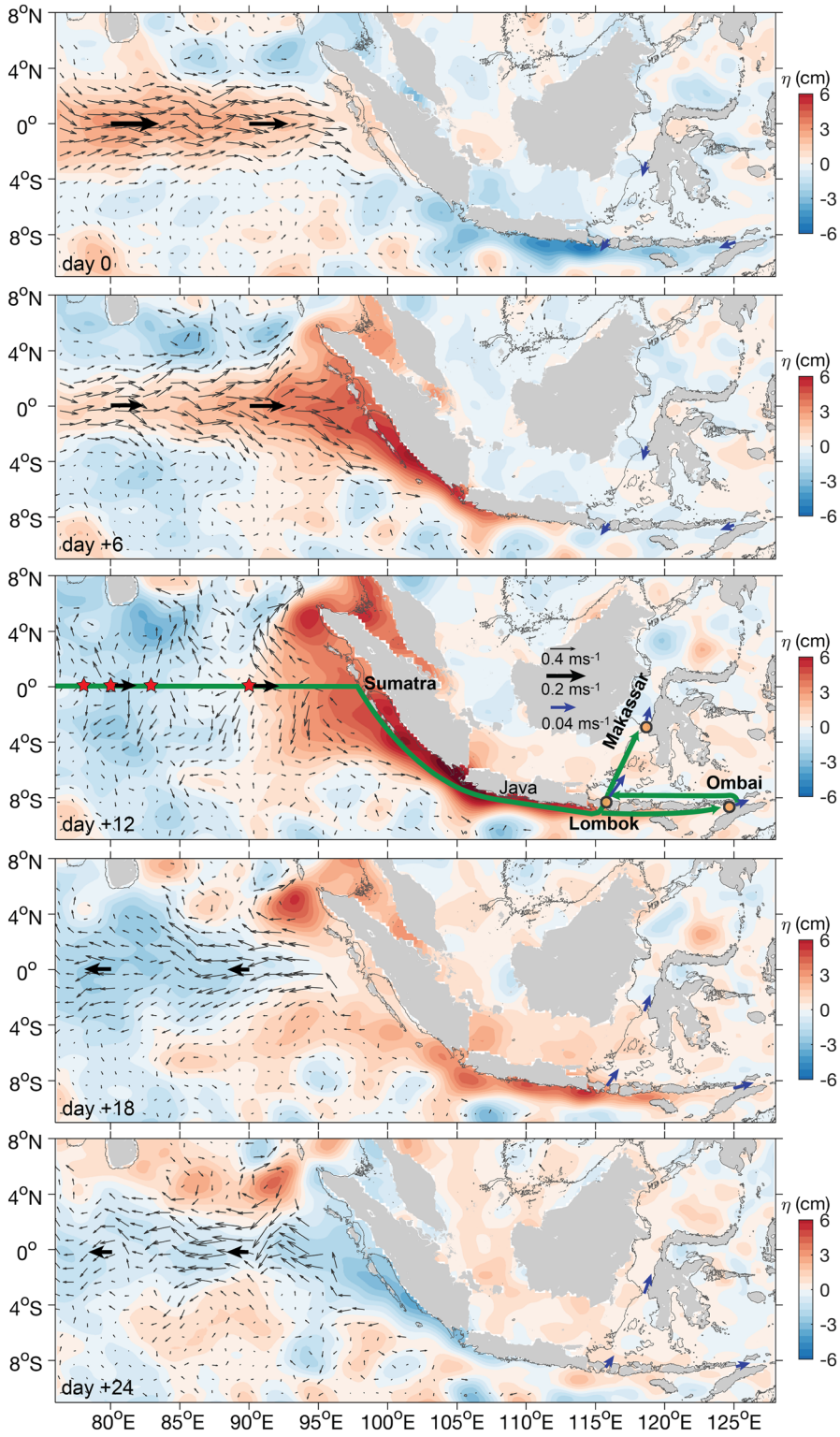

Figure 8. Composites of intraseasonal η and OSCAR surface currents (thin black arrows) attributed to Kelvin wave passage observed during August 2008–July 2013 across the central Indian Ocean - Maritime continent region for days between day = 0 and day = +24, with day = 0 marking the time when η and u_r are maximum at 0°, 80.5° E. Thick black arrows indicate u_r averaged in the upper 100 m at 80.5 and 90° E, while blue arrows indicate v_r' averaged in the upper 100 m in Lombok Strait and between 100 and 200 m in Makassar Strait, and u_r' averaged between 100 and 200 m in Ombai Strait. Green arrows indicate plausible waveguides from the equatorial Indian Ocean to the Indonesian seas. Red stars and brown dots mark the mooring locations along the waveguides. Contours denote an isobath of 100 m.

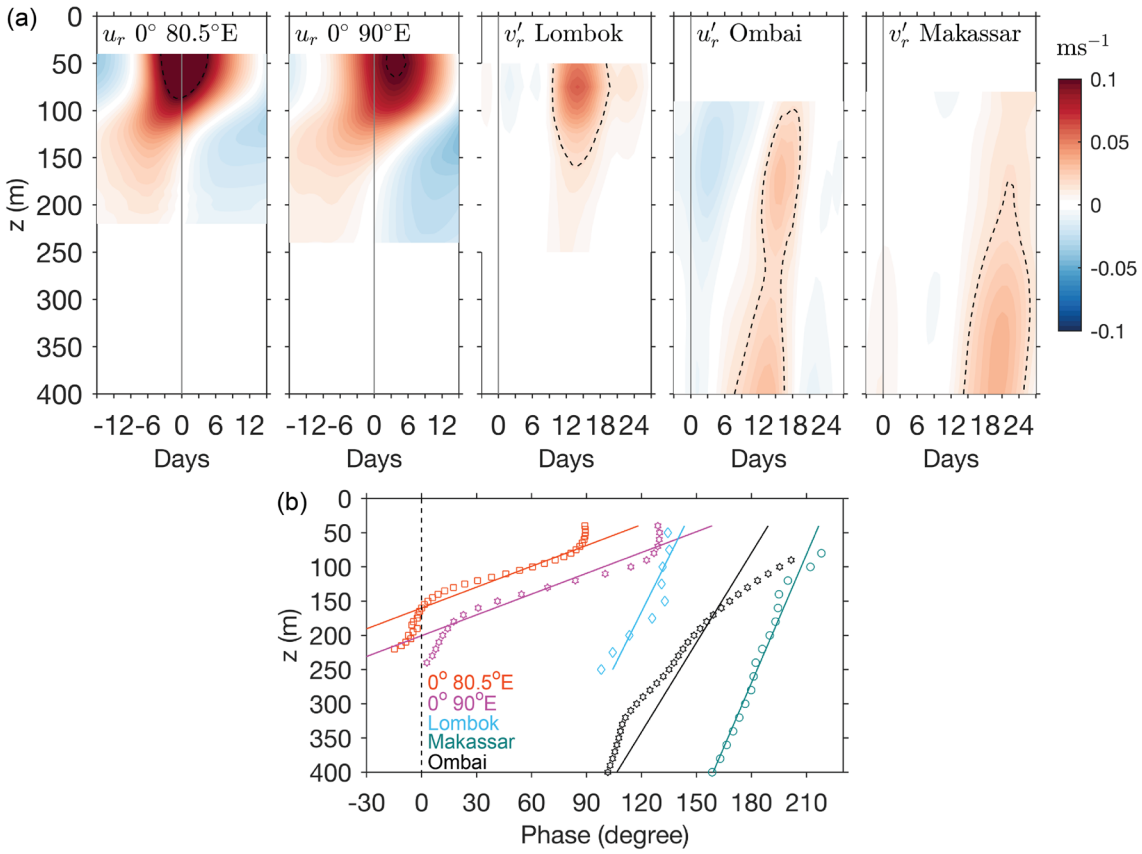

Figure 9. (a) Composites of u_r at 0°, 80.5° E and 0°, 90° E and along-strait velocity in Lombok, Makassar, and Ombai straits attributed to passages of Kelvin wave observed during October 2004–December 2006; dashed contours mark $u_r = 0.2$ ms^{-1} at the equatorial moorings and along-strait velocity of 0.02 ms^{-1} at the Indonesian straits. Positive values in Lombok and Makassar straits indicate northward flow, while those in Ombai Strait indicate northeastward flow. (b) CEOF phases of u_r and along-strait velocity; values increasing to the Indonesian straits and upward, respectively, indicate eastward and upward phase propagation. The phase at each mooring site is referenced to that at 0°, 80.5° E at 160 m. Color-coded lines show the linear least-squares fits to the CEOF phases across depths beneath 50 m.

the difference. The mean N averaged across the water column deeper than 200 m in the Indonesian straits is roughly a third of that averaged in the upper 200 m along the equatorial Indian Ocean, based on CTD casts near the RAMA and ITF moorings. Consistent with characteristics of linear equatorial Kelvin waves propagating upward at a faster speed in a less stratified water column, weaker stratification may favor faster upward propagation of Kelvin waves in the Indonesian straits.

To further showcase propagation of Indian Ocean Kelvin waves into the Indonesian seas, we regressed the reconstructed along-strait velocity in Makassar Strait to the basin scale η and τ across the Indian Ocean and the Indonesian seas, complementing the results inferred from composite analysis of the point-based measurements. Scaled to one standard deviation of the depth-averaged time series between 100 and 200 m in Makassar Strait series, time-evolution of regressed η and τ clearly depicts the basin-scale feature of the Indian Ocean Kelvin wave (Figure 10).

At lag 0 day, marked with the maximum magnitude of the downwelling Kelvin wave-forced northward v_r' in Makassar Strait, the η and τ fields over the central equatorial Indian Ocean are respectively suppressed and easterly, marking the onset of the upwelling Kelvin wave there. The preceding sequences demonstrate the evolution of η attributed to the downwelling Kelvin wave, from the wave onset responding to westerlies over the equatorial Indian Ocean to the η propagation along the southern coasts of Indonesian archipelago.

Composited and regressed η illustrate that equatorial Indian Ocean Kelvin waves propagate along the southern coasts of Sumatra and Java and penetrate into the Indonesian straits as coastally or topographically trapped waves (Figures 8 and 10). In a rotating and inviscid fluid, a horizontally bounded domain such as a channel and strait could sustain propagation of Kelvin and Poincaré waves (Pedlosky, 2013). In contrast to

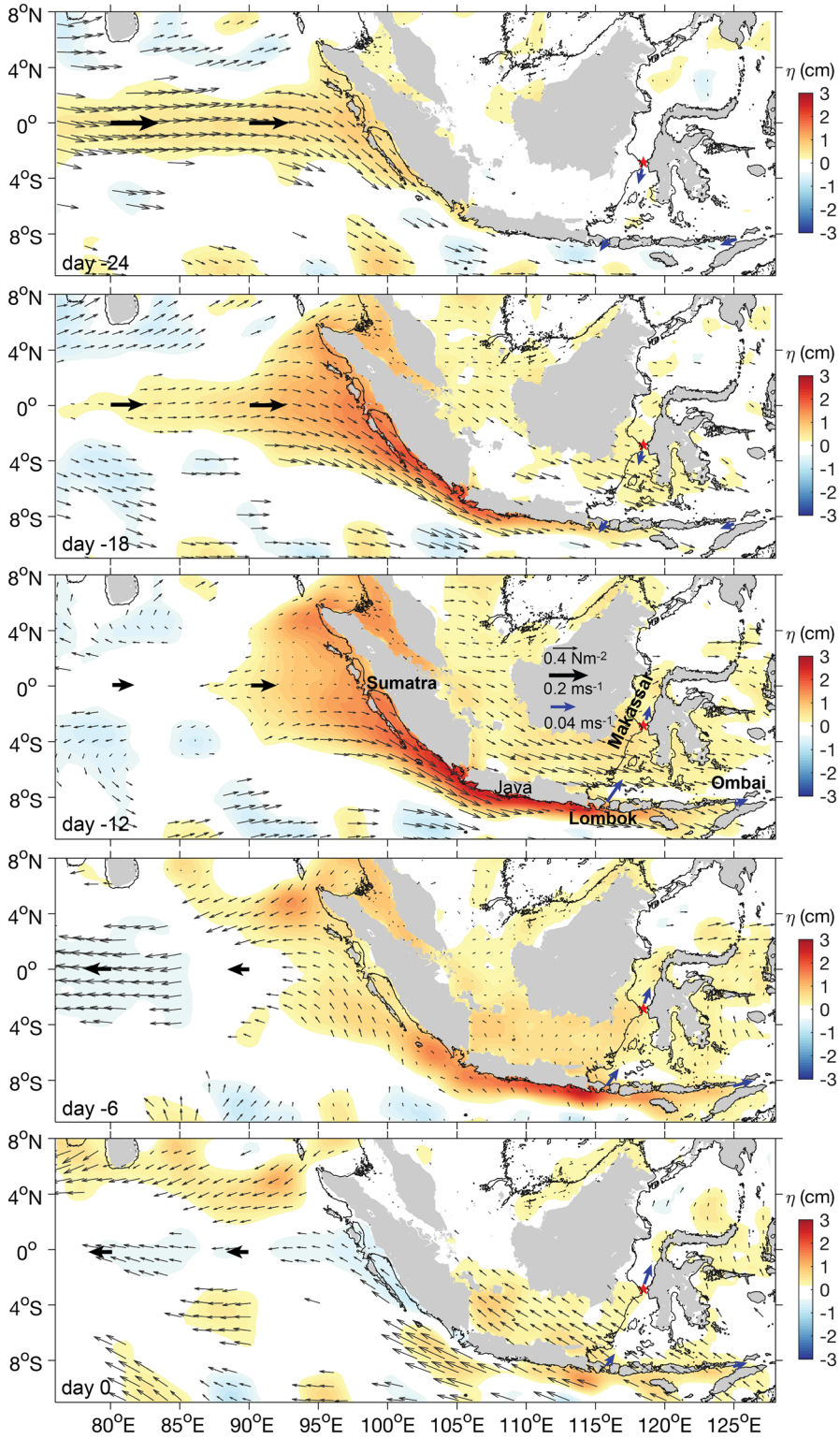

Figure 10. Intraseasonal η and τ (thin black arrows) regressed against v_r' averaged between 100 and 200 m in Makassar Strait for lags between −24 days and 0 day scaled to one standard deviation of v_r'. Only regressions significant at 80% level are shown. Negative lags imply η and τ lead. The regression analyses used the observations during January 2004–July 2011 and August 2013–December 2016. Red star indicates Makassar Strait mooring site. Contours show an isobath of 100 m. Thick black arrows indicate u_r averaged in the upper 100 m at 80.5° E and 90° E, while blue arrows indicate v_r' averaged in the upper 100 m in Lombok Strait and between 100 and 200 m in Makassar Strait and u_r' averaged between 100 and 200 m in Ombai Strait.

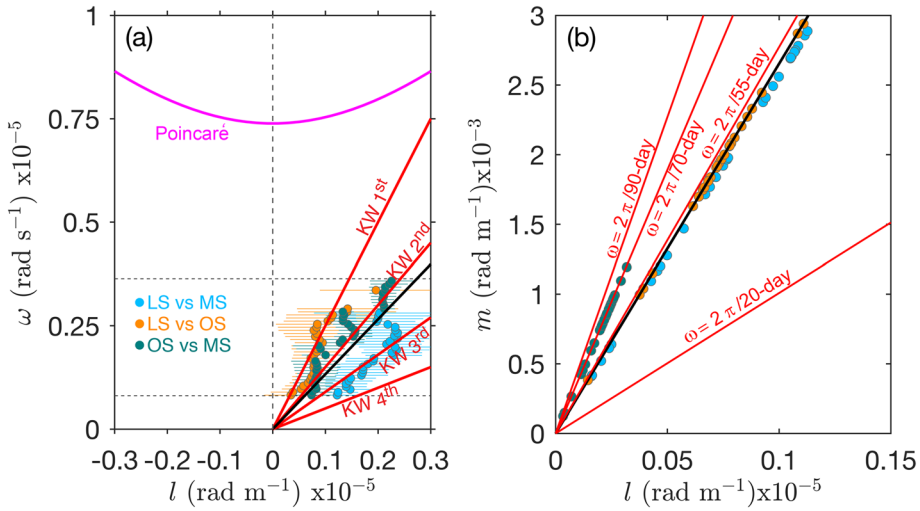

Figure 11. Dispersion diagrams of (a) the wave frequency versus the horizontal wavenumber, l, and (b) the vertical wavenumber, m, versus l inferred from coherence analyses of the reconstructed intraseasonal along-strait velocities in Lombok Strait (LS), Makassar Strait (MS), and Ombai Strait (OS). Color-coded dots indicate the observed dispersion estimates, magenta curve in (a) denotes the theoretical dispersion curve for Poincaré wave, red lines in (a) indicate the first four baroclinic Kelvin wave dispersion curves, and red lines in (b) denote theoretical dispersion curves of the Kelvin waves for four different intraseasonal frequencies. Reconstructed velocities at 200 m in all straits are used to derive the dispersion diagram shown in (a), while the velocities at 100 m in LS and at 500 m in MS and OS are used for (b). Black lines indicate linear least-squares fits of the inferred dispersion diagrams and are associated respectively with $c = 1.3 \pm 0.2$ ms^{-1} for (a) and $\omega = 2\pi/(52 \pm 2)$ days for (b). We assume Kelvin wave paths (mid panel of Figure 8) to derive the dispersion diagrams. Color-coded horizontal lines in (a) indicate 95% confidence level for the wavenumber-frequency plots, estimated based on a Monte Carlo method. Horizontal dashed black lines mark the intraseasonal frequency band.

the unidirectional and nondispersive Kelvin waves, Poincaré waves are dispersive and propagate in either direction along a strait or channel. The intraseasonal reconstructed along-strait velocities are coherent in Lombok, Ombai, and Makassar straits, with a significant average squared coherence amplitude of 0.62 ± 0.09 and phase lags indicating propagation into Makassar Strait. Inferred from the phase lags, the horizontal wavenumber-frequency estimates (color-coded dots in Figure 11a) span the range of theoretical dispersion curves for the lowest three vertical mode Kelvin waves, with propagation from Lombok to Makassar Strait (blue), Lombok to Ombai Strait (orange), and Ombai to Makassar Strait (green). These estimates fall well outside the range Poincaré waves, $\omega = \sqrt{f^2 + c^2 l^2}$, with l denoting the horizontal wavenumber and c set to 1.3 ms^{-1} (Figure 11a).

The Kelvin wave dispersion diagrams estimates are consistent with the results of previous intraseasonal Kelvin wave studies reporting propagations of intraseasonal Kelvin waves from Lombok Strait to each of Ombai Strait (Drushka et al., 2010) and Makassar Straits (Pujiana et al., 2013). Overall, like in the equatorial Indian Ocean, the linear least-squares fit on the ω - l plane (black line in Figure 11a) reveals a regression slope consistent with a second baroclinic mode phase speed of 1.3 ± 0.2 ms^{-1}. Although the uncertainties in these estimates are large, the wave speeds on the Lombok-Makassar path however are slower than on the other paths and closer to that of the third baroclinic mode.

The Kelvin waves not only propagate horizontally but also vertically into the Indonesian straits, evident in the vertical phase shift shown by the composites of the along-strait velocities (Figure 9). As the equatorial Kelvin wave, a coastal Kelvin wave maintains its nondispersive nature, such that ω is proportional to l. For a vertically propagating coastal Kelvin wave at low latitudes, Romea and Allen (1983) suggested a dispersion relation of $\omega = \frac{N}{|m|} l$, where m is vertical wavenumber. By setting $N = 3.7\times 10^{-3}$ s^{-1}, the depth-averaged value of N in the upper 500 m from CTD casts near the ITF mooring sites, and performing a coherence analysis of the intraseasonal reconstructed along-strait velocities in Lombok, Makassar, and Ombai straits, we derived a set of vertical and horizontal wavenumbers. These wavenumbers agree with the dispersion of vertically propagating coastal Kelvin waves oscillating at intraseasonal frequencies (Figure 11b). The linear least-squares fit to the observed dispersion relation estimates (black line in Figure 11b), with the inferred

$\omega = 2\pi/(52 \pm 2)$ days, matches the theoretical dispersion curve for a coastal Kelvin wave recurring with a frequency of $2\pi/55$ day. This further supports our hypothesis that Kelvin waves predominantly account for intraseasonal variations of the along-strait velocity in the Indonesian straits.

4. Summary and Discussion

We describe the modal structure and propagation of intraseasonal Kelvin waves along a waveguide stretching from the central equatorial Indian Ocean to the Indonesian seas using in situ horizontal current data from an array of fourteen moored ADCPs combined with satellite-derived sea level and surface zonal current anomaly data over the period of 2004–2016. To identify Kelvin wave events from the observations, we decomposed the intraseasonal η data along the equatorial Indian Ocean into CEOF modes and reconstructed η (η_r) based on the first CEOF mode (which accounts for 58% of the intraseasonal η variance and exhibits eastward propagation). We then traced the propagation of these waves along the coast of Indonesia and into the Indonesian seas using a variety of methods. The main results are as follows.

1. We identified 65 downwelling and 57 upwelling intraseasonal Kelvin waves in the equatorial Indian Ocean during the observational period. The composite of sea level associated with each of the Kelvin wave groups shows that the downwelling and upwelling Kelvin waves share common characteristics in their zonal evolution along the equator, implying that the results from the analysis of downwelling Kelvin waves should be applicable to upwelling Kelvin waves as well appropriately accounting for sign changes.
2. The depth-averaged zonal velocity in the upper 220 m, satellite-retrieved sea level and surface geostrophic flow along 80.5° E are most energetic on the equator and decay poleward. The least-squares exponential fits to the depth-averaged zonal velocity, and the satellite data closely approximate the theoretical cross-equatorial structure of zonal current and sea level associated with equatorial Kelvin waves. Phase speeds inferred from the least-squares fits and the ratio of surface pressure to surface zonal geostrophic current at the equator are of 1.3–1.4 ms^{-1}, indicating the predominance of the second baroclinic mode Kelvin wave with a latitudinal decay scale of ~250 km.
3. Composites of zonal velocity from the equatorial Indian Ocean moorings illustrate a coherent vertical structure that horizontally propagates towards the west coast of Sumatra. The wavenumber-frequency spectrum inferred from the intraseasonal zonal velocity variability compares well with the theoretical dispersion curve for equatorial Kelvin waves, consistent with the dominance of the second baroclinic mode. Moreover, there is consistent upward phase shift along the equator, implying downward energy propagation as the Kelvin waves propagate eastward.
4. Composites of sea level and surface current during the Kelvin wave events illustrate the basin-scale evolution of the wave. Equatorial intraseasonal Kelvin waves propagate eastward, encounter the west coast of Sumatra, and then continue poleward as coastal Kelvin waves along Sumatra and Java. Regressed sea level against the reconstructed along-strait velocity in Makassar Strait provides a consistent picture of the variability. It takes about 24 days for intraseasonal Kelvin waves to complete a half cycle, consistent with the 55-day central period of the oscillation. The coastal Kelvin waves also generate reflected Rossby waves around 5° N and 5° S off the coast of Sumatra.
5. Composites of intraseasonal along-strait velocities in Lombok, Makassar, and Ombai straits during equatorial Kelvin wave events highlight the penetration of wave energy into the Indonesian seas. The Kelvin wave signals arrive subsequently at Lombok, Ombai, and Makassar straits within a 24-day period following their genesis in the central Indian Ocean. The wave dispersion, deduced from coherent along-strait velocities, is consistent with Kelvin wave dynamics.

Evaluation of the meridional zonal current structure from moorings and from satellite-derived sea level and surface geostrophic flow anomalies during the passage of intraseasonal Kelvin waves in the Indian Ocean provide a new insight into not only the meridional structure of the Kelvin wave but also the wave's baroclinic structure. Observed vertical phase propagation suggests the presence of the first two lowest baroclinic modes, with the second mode dominating. The significance of the second baroclinic mode in governing zonal current variations in the equatorial Indian Ocean at intraseasonal, seasonal, and interannual timescales has been reported in previous studies (Han et al., 2011; Nagura & McPhaden, 2010a, 2010b, 2012).

Our study highlights the direct connection between equatorial Kelvin waves in the Indian Ocean and coastally trapped Kelvin waves in Lombok and Ombai straits using the simultaneously observed ocean current velocities. We extend the results of the previous studies by establishing the direct connection between

equatorial Kelvin waves and topographically trapped Kelvin waves in Makassar Strait from observations, corroborating the study of Pujiana et al. (2013) that reported characteristics of intraseasonal Kelvin waves propagating from Lombok to Makassar Strait. This is in contrast to Iskandar et al. (2005) and Zhou and Murtugudde (2010), who found that Kelvin waves did not penetrate into Makassar Strait. Our results, supported by the along-strait velocity derived dispersion diagrams, suggest that intraseasonal Kelvin waves in Ombai Strait likely penetrate into Banda Sea and subsequently propagate westward along the northern coast of lesser Sunda islands and northward into Makassar Strait, while Schiller et al. (2010) suggested that Kelvin waves dissipated in Banda Sea. Unlike the other Kelvin wave paths between Lombok-Makassar and Lombok-Ombai Strait, the Ombai-Makassar Strait path is less certain since there are no intermediate observations between the two straits. The dispersion diagram for the Ombai-Makassar station pair, suggesting a distinct 70-day period, is dependent upon this assumed path. Despite large uncertainties, the dispersion diagrams also indicate that the Kelvin waves propagating at a slower speed along the Lombok-Makassar path than along the Lombok-Ombai path, with the reasons for the slower speed unclear.

Local wind stresses appear to be less influential in determining the velocity patterns at intrasesonal timescales in the Indonesian straits. Based on the regressed wind stress fields shown in Figure 10, the period during which the signature of downwelling Kelvin waves is most pronounced in the straits coincides with east-southeasterly winds across the Indonesian seas, unfavorable for generating Kelvin waves. The southeasterly wind stress drives southward surface Ekman flow in Makassar and Lombok straits and south-westward Ekman flow in Ombai Strait, counteracting the Kelvin wave flows along the straits. In Makassar Strait, particularly, local wind stress fluctuations would not be an effective source of intraseasonal variability at depths of 150 m and deeper since the local mixed layer and presumably Ekman layer is shallower than 50–75 m (Pujiana et al., 2009).

Although the impact of local intraseasonal wind stress forcing of Kelvin waves in Makassar Strait is likely to be negligible, southeasterly wind stress variations could drive Ekman convergence along the northern coast of lesser Sunda islands. Ekman convergence would set favorable conditions for the generation of downwelling Kelvin waves, which then might propagate into Makassar Strait. A more quantitative evaluation of the role of local winds in the Indonesian seas versus remote winds in the Indian Ocean in forcing Kelvin waves in Makassar Strait requires numerical experiments which are beyond the scope of the present study.

The role of Kelvin waves in connecting the ubiquitous intraseasonal variability of ocean currents in the equatorial Indian Ocean and the Indonesian straits is clear from the observations. Indian Ocean Kelvin waves may also affect sea surface temperature (SST) in the Indonesian seas, where the SST shows pronounced intraseasonal variability (Napitu et al., 2015). Napitu et al. (2015) quantified the degree of SST coupling with MJO surface heat fluxes in the Indonesian seas but not yet with possible oceanic processes such as Kelvin waves. The contribution of Indian Ocean-forced Kelvin waves in vertically distributing heat from the surface to deeper depths and hence affecting heat flux transferred from the Pacific to the Indian Ocean via the Indonesian throughflow remains open questions.

Acknowledgments
We thank two anonymous reviewers for their thoughtful and constructive comments on earlier versions of this manuscript. We acknowledge NOAA and its partners for maintaining the RAMA moored buoy array and appreciate important contributions of Ministry of Marine Affairs and Fisheries of the Republic of Indonesia, Drs Arnold Gordon and Asmi Napitu for arrangements to service the Makassar Strait mooring. Gratitude is extended to Dr Janet Sprintall for sharing the mooring data in Lombok and Ombai straits. RAMA data can be downloaded via https://www.pmel.noaa.gov/tao/drupal/disdel/, and the ITF data can be obtained from http://ocp.ldeo.columbia.edu/res/div/ocp/projects/MITF/cm_data/ and http://www.marine.csiro.au/~cow074/instantdata.htm. The satellite-derived and OSCAR current data are available in http://marine.copernicus.eu/services-portfolio/access-to-products/ and http://apdrc.soest.hawaii.edu/datadoc/podaac_oscar.php. The Argo profile data can be obtained from http://www.argodatamgt.org/Access-to-data/Argo-data-selection. This research was performed while the first author held a National Research Council Research Associateship Award at NOAA/PMEL. MJM is supported by NOAA. This is PMEL contribution 5012.

References

Arief, D., & Murray, S. P. (1996). Low-frequency fluctuations in the Indonesian throughflow through Lombok Strait. *Journal of Geophysical Research*, *101*(C5), 12,455–12,464.

Bonjean, F., & Lagerloef, G. S. (2002). Diagnostic model and analysis of the surface currents in the tropical Pacific Ocean. *Journal of Physical Oceanography*, *32*(10), 2938–2954.

Boulanger, J. P., & Menkes, C. (1995). Propagation and reflection of long equatorial waves in the Pacific Ocean during the 1992–1993 El Niño. *Journal of Geophysical Research*, *100*(C12), 25,041–25,059. https://doi.org/10.1029/95JC02956

Drushka, K., Sprintall, J., Gille, S. T., & Brodjonegoro, I. (2010). Vertical structure of Kelvin waves in the Indonesian throughflow exit passages. *Journal of Physical Oceanography*, *40*(9), 1965–1987.

Durland, T. S., & Qiu, B. (2003). Transmission of subinertial Kelvin waves through a strait. *Journal of Physical Oceanography*, *33*(7), 1337–1350.

Gordon, A. L., Sprintall, J., Van Aken, H. M., Susanto, D., Wijffels, S., Molcard, R., et al. (2010). The Indonesian throughflow during 2004–2006 as observed by the INSTANT program. *Dynamics of Atmospheres and Oceans*, *50*(2), 115–128.

Han, W., Lawrence, D., & Webster, P. (2001). Dynamical response of equatorial Indian Ocean to intraseasonal winds: Zonal flow. *Geophysical Research Letters*, *28*(22), 4215–4218.

Han, W., McCreary, J. P., Masumoto, Y., Vialard, J., & Duncan, B. (2011). Basin resonances in the equatorial Indian Ocean. *Journal of Physical Oceanography*, *41*(6), 1252–1270. https://doi.org/10.1175/2011jpo4591.1

Iskandar, I., Mardiansyah, W., Masumoto, Y., & Yamagata, T. (2005). Intraseasonal Kelvin waves along the southern coast of Sumatra and Java. *Journal of Geophysical Research*, *110*, C04013. https://doi.org/10.1029/2004JC002508

Iskandar, I., & McPhaden, M. J. (2011). Dynamics of wind-forced intraseasonal zonal current variations in the equatorial Indian Ocean. *Journal of Geophysical Research*, *116*, C06019. https://doi.org/10.1029/2010JC006864

Johnson, E. S., & McPhaden, M. J. (1993). Structure of intraseasonal Kelvin waves in the equatorial Pacific Ocean. *Journal of Physical Oceanography*, *23*(4), 608–625.
Kessler, W. S., Mcphaden, M. J., & Weickmann, K. M. (1995). Forcing of intraseasonal Kelvin waves in the equatorial Pacific. *Journal of Geophysical Research*, *100*(C6), 10,613–10,631. https://doi.org/10.1029/95JC00382
Luyten, J. R., & Roemmich, D. H. (1982). Equatorial currents at semi-annual period in the Indian Ocean. *Journal of Physical Oceanography*, *12*(5), 406–413.
Masumoto, Y., Hase, H., Kuroda, Y., Matsuura, H., & Takeuchi, K. (2005). Intraseasonal variability in the upper layer currents observed in the eastern equatorial Indian Ocean. *Geophysical Research Letters*, *32*, L02607. https://doi.org/10.1029/2004GL021896
McCreary, J. P. (1984). Equatorial beams. *Journal of Marine Research*, *42*(2), 395–430.
McPhaden, M. J. (1982). Variability in the central equatorial Indian Ocean. 1. Ocean dynamics. *Journal of Marine Research*, *40*(1), 157–176.
McPhaden, M. J., Meyers, G., Ando, K., Masumoto, Y., Murty, V. S. N., Ravichandran, M., et al. (2009). RAMA: The research moored array for African-Asian-Australian monsoon analysis and prediction. *Bulletin of the American Meteorological Society*, *90*(4), 459–480.
McPhaden, M. J., Wang, Y., & Ravichandran, M. (2015). Volume transports of the Wyrtki jets and their relationship to the Indian Ocean Dipole. *Journal of Geophysical Research: Oceans*, *120*, 5302–5317. https://doi.org/10.1002/2015JC010901
Nagura, M., & McPhaden, M. J. (2010a). Dynamics of zonal current variations associated with the Indian Ocean Dipole. *Journal of Geophysical Research*, *115*, C11026. https://doi.org/10.1029/2010JC006423
Nagura, M., & McPhaden, M. J. (2010b). Wyrtki jet dynamics: Seasonal variability. *Journal of Geophysical Research*, *115*, C07009. https://doi.org/10.1029/2009JC005922
Nagura, M., & McPhaden, M. J. (2012). The dynamics of wind-driven intraseasonal variability in the equatorial Indian Ocean. *Journal of Geophysical Research*, *117*, C02001. https://doi.org/10.1029/2011JC007405.
Nagura, M., & McPhaden, M. J. (2014). Zonal momentum budget along the equator in the Indian Ocean from a high-resolution ocean general circulation model. *Journal of Geophysical Research: Oceans*, *119*, 4444–4461. https://doi.org/10.1002/2014JC009895
Nagura, M., & McPhaden, M. J. (2016). Zonal propagation of near-surface zonal currents in relation to surface wind forcing in the equatorial Indian Ocean. *Journal of Physical Oceanography*, *46*(12), 3623–3638. https://doi.org/10.1175/Jpo-D-16-0157.1
Napitu, A. M., Gordon, A. L., & Pujiana, K. (2015). Intraseasonal sea surface temperature variability across the Indonesian Seas. *Journal of Climate*, *28*(22), 8710–8727.
Pedlosky, J. (2013). *Waves in the ocean and atmosphere: Introduction to wave dynamics*: Springer Science & Business Media.
Pujiana, K., Gordon, A. L., Metzger, E. J., & Ffield, A. L. (2012). The Makassar Strait pycnocline variability at 20–40 days. *Dynamics of Atmospheres and Oceans*, *53*, 17–35.
Pujiana, K., Gordon, A. L., & Sprintall, J. (2013). Intraseasonal Kelvin wave in Makassar Strait. *Journal of Geophysical Research: Oceans*, *118*, 2023–2034. https://doi.org/10.1002/jgrc.20069
Pujiana, K., McPhaden, M. J., Gordon, A. L., & Napitu, A. M. (2019). Unprecedented response of Indonesian throughflow to anomalous Indo-Pacific climatic forcing in 2016. *Journal of Geophysical Research: Oceans*, *124*, 3737–3754. https://doi.org/10.1029/2018JC014574
Pujiana, K., Gordon, A. L., Sprintall, J., & Susanto, R. D. (2009). Intraseasonal variability in the Makassar Strait thermocline. *Journal of Marine Research*, *67*(6), 757–777.
Romea, R., & Allen, J. (1983). On vertically propagating coastal Kelvin waves at low latitudes. *Journal of Physical Oceanography*, *13*(7), 1241–1254.
Schiller, A., Wijffels, S., Sprintall, J., Molcard, R., & Oke, P. R. (2010). Pathways of intraseasonal variability in the Indonesian throughflow region. *Dynamics of Atmospheres and Oceans*, *50*(2), 174–200.
Sengupta, D., Senan, R., & Goswami, B. N. (2001). Origin of intraseasonal variability of circulation in the tropical central Indian Ocean. *Geophysical Research Letters*, *28*(7), 1267–1270. https://doi.org/10.1029/2000GL012251
Sengupta, D., Senan, R., Murty, V. S. N., & Fernando, V. (2004). A biweekly mode in the equatorial Indian Ocean. *Journal of Geophysical Research*, *109*, C10003. https://doi.org/10.1029/2004JC002329
Smyth, W. D., Durland, T. S., & Moum, J. N. (2015). Energy and heat fluxes due to vertically propagating Yanai waves observed in the equatorial Indian Ocean. *Journal of Geophysical Research: Oceans*, *120*, 1–15. https://doi.org/10.1002/2014JC010152
Sprintall, J., Wijffels, S. E., Molcard, R., & Jaya, I. (2009). Direct estimates of the Indonesian Throughflow entering the Indian Ocean: 2004-2006. *Journal of Geophysical Research*, *114*, C07001. https://doi.org/10.1029/2008JC005257
Sprintall, J., Wijffels, S., Molcard, R., & Jaya, I. (2010). Direct evidence of the South Java current system in Ombai Strait. *Dynamics of Atmospheres and Oceans*, *50*(2), 140–156.
Syamsudin, F., Kaneko, A., & Haidvogel, D. B. (2004). Numerical and observational estimates of Indian Ocean Kelvin wave intrusion into Lombok Strait. *Geophysical Research Letters*, *31*, L24307. https://doi.org/10.1029/2004GL021227
Yan, D., Kai, L., Wei, Z., & Wei-Dong, Y. (2012). The Kelvin wave processes in the equatorial Indian Ocean during the 2006–2008 IOD events. *Atmospheric and Oceanic Science Letters*, *5*(4), 324–328.
Yoneyama, K., Zhang, C., & Long, C. N. (2013). Tracking pulses of the Madden–Julian oscillation. *Bulletin of the American Meteorological Society*, *94*(12), 1871–1891.
Yu, X., & McPhaden, M. J. (1999). Seasonal variability in the equatorial Pacific. *Journal of Physical Oceanography*, *29*(5), 925–947.
Zhang, C. D. (2013). Madden–Julian oscillation bridging weather and climate. *Bulletin of the American Meteorological Society*, *94*(12), 1849–1870. https://doi.org/10.1175/Bams-D-12-00026.1
Zhou, L., & Murtugudde, R. (2010). Influences of Madden–Julian oscillations on the eastern Indian Ocean and the maritime continent. *Dynamics of Atmospheres and Oceans*, *50*(2), 257–274.